ACTIVE MEDIA

Structural, optical, and spectroscopic properties and efficient two-micron lasing of new $Tm^{3+}:Lu_2O_3$ ceramics

O.L. Antipov, S.Yu. Golovkin, O.N. Gorshkov, N.G. Zakharov, A.P. Zinov'ev, A.P. Kasatkin, M.V. Kruglova, M.O. Marychev, A.A. Novikov, N.V. Sakharov, E.V. Chuprunov

Abstract. The structural, optical, and spectroscopic properties of new $Tm^{3+}:Lu_2O_3$ laser ceramics are studied. The average size of a ceramic grain (crystallite) is found to be 540–560 nm. The absorption spectrum measured in the near-IR region shows that this ceramics can be pumped by commercially available laser diodes at wavelengths of 796 and 811 nm. The high-transmission region of the ceramics in the mid-IR region extends to 7 μm. Investigations of the luminescence spectrum in the region of 1.75–2.2 μm upon laser-diode pumping show strong lines peaked at wavelengths of 1942, 1965, and 2066 nm. Ellipsometric measurements yield refractive indices $n \approx 1.92$ at the pump wavelength 796 nm and $n \approx 1.94$ at the laser wavelength 2066 nm. Continuous-wave lasing of a $Tm^{3+}:Lu_2O_3$ ceramic laser at a wavelength of 2066 nm is demonstrated under diode-laser pumping at wavelengths of 796 and 811 nm.

1. Introduction

The two-micron (1.9–2.1 μm) lasers are widely used in medicine (surgery, urology, ophthalmology, angioplasty, arthroscopy, etc.), remote probing of the atmosphere, ecological monitoring, plastic processing, and other fields [1–3]. In addition, lasers emitting at wavelength $\lambda > 2$ μm are ideal sources for pumping mid-IR (3–6 μm) optical parametric oscillators (OPOs) based on, for example, $ZnGeP_2$ crystals [4].

At present, two-micron laser radiation is obtained using lasers based on Ho^{3+}- and/or Tm^{3+}-doped crystals or silica fibres [1, 5, 6]. An advantage of holmium solid-state and fibre lasers is that they can operate at long wavelengths (at $\lambda \sim 2.1$ μm), but, for efficient pumping of these lasers, it is necessary to use radiation at $\lambda \sim 1.9$ μm, which requires creation of special pump lasers. Thulium lasers, in which the upper laser level is populated by cross-relaxation, can be pumped by diodes with $\lambda \sim 800$ nm [5]. However, these lasers operate, as

a rule, at a wavelength shorter than 2 μm, which limits the field of their application (for example, in OPOs).

In recent publications, it was reported on diode-pumped ($\lambda = 796$ nm) lasers based on thulium-doped sesquioxide crystals $Tm^{3+}:Lu_2O_3$ and $Tm^{3+}:Sc_2O_3$, which demonstrated efficient high-power lasing at $\lambda = 2065$ and 2116 nm, respectively [1, 7–9]. Unfortunately, these single crystals are difficult to produce (by the Kyropoulos or heat-exchange methods) due to a high melting temperature ($\sim 2450\,°C$), and, at present, are grown only in one laboratory in the world (Institute of Laser Physics, University of Hamburg, Germany) [1, 7–10]. An alternative method of production of sesquioxide active elements is sintering of ceramics. To date, there exist lasers based on Lu_2O_3, Sc_2O_3, and Y_2O_3 sesquioxide ceramics doped with Nd^{3+}, Yb^{3+}, and Ho^{3+} ions [11–20].

The present work is devoted to the study of the structural, optical, and spectroscopic properties of new $Tm^{3+}:Lu_2O_3$ laser ceramics, which is produced for the first time by Konoshima Chemicals Co. (Japan) by our request. We also study lasing in this ceramics.

2. Study of the ceramic structure using a scanning electron microscope

We studied the structure of grains (crystallites) in $Tm^{3+}:Lu_2O_3$ ceramic samples (with a thulium concentration of 2 at.%) in the form of cylindrical plates ~ 3 mm thick and 20 mm in diameter with both faces polished (Fig. 1). The study was performed using a Jeol JSM-6490 (Jeol, Japan) scanning electron microscope.
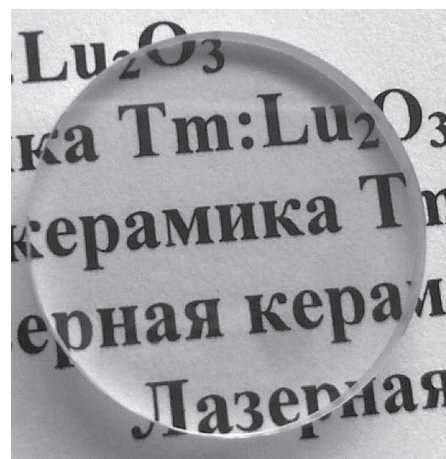

Figure 1. Photograph of a ceramic sample.

O.L. Antipov, S.Yu. Golovkin, N.G. Zakharov, A.P. Zinov'ev, A.A. Novikov Institute of Applied Physics, Russian Academy of Sciences, ul. Ul'yanova 46, 603950 Nizhnii Novgorod, Russia; e-mail: antipov@appl.sci-nnov.ru;
O.N. Gorshkov, A.P. Kasatkin, M.V. Kruglova, M.O. Marychev, N.V. Sakharov, E.V. Chuprunov N.I. Lobachevsky Nizhnii Novgorod State University, prosp. Gagarina 23, 603950 Nizhnii Novgorod, Russia; e-mail: gorshkov@phys.unn.ru
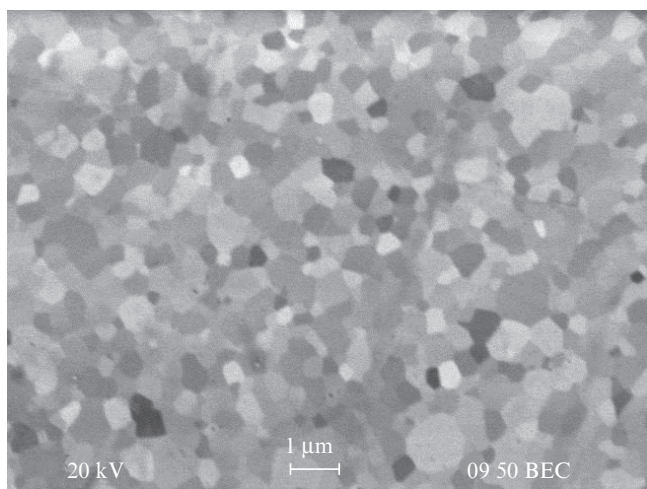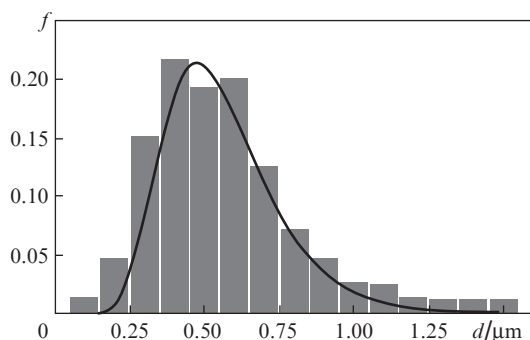
The samples were attached to a substrate by a conductive adhesive tape without special procedures for removing electrostatic charges. This ensured the absence of distortions of information that could be caused by deposition of a conducting layer. Note that the electron-beam charging of samples leads to light-striking of some regions of the sample, which negatively affects the total image quality. To minimise this effect, the samples were photographed at the minimum accelerating voltage and spot size to ensure a required resolution.

The obtained images allow us to reveal the structural features of the studied ceramic samples (Fig. 2). It is known that the Lu_2O_3 crystal has a cubic crystal lattice [10]. The visible differences in the electron microscope signals can be caused by random orientations of crystallographic axes in ceramic crystallites.

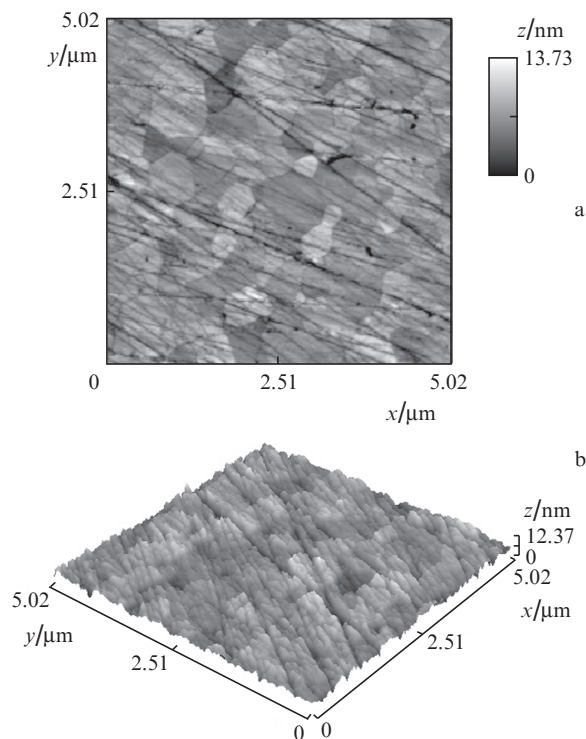$$f(d) = \frac{\alpha}{\sigma d \sqrt{2\pi}} \exp\left[-\frac{(\ln d - \mu)^2}{2\sigma^2}\right], \tag{1}$$

where d is the grain size in micrometers; $\alpha = 0.0915$; $\mu = -0.59$; and $\sigma = 0.34$. The histogram of the grain size distribution and the approximating function are presented in Fig. 3. The average grain size determined by the maximum of distribution (1) is ~ 535 nm.

## 3. Investigation of the ceramics structure with an atomic force microscope

The surface morphology of the ceramics was studied using a Solver Pro (NT-MDT, Zelenograd, Russia) atomic-force microscope (AFM). These investigations were performed under atmospheric conditions in a contact regime using NSG01-DLC (NT-MDT) silicon cantilevers with the nominal tip radius of curvature $R < 3$ nm. The maximum resolution of the AFM measurements was 3 nm in the surface plane and 1 nm in height. The AFM data were processed using special softwares C3M NT-MDT Nova Image Analysis 2.0 and SPMLab Analysis Only 5.01 (Veeco Instruments, US).

Before the measurements, the sample surface was etched for 10 min in a $1:2$ $HF-HNO_3$ acid mixture heated to $60\,°C$.

Based on processed AFM images of the surface, we calculated the average grain size and its rms deviation and plotted the grain size distributions (Figs 4, 5). To calculate the average grain size, we used the same chord length measurement method [21]. The grain size distribution was also approximated by the log-normal distribution function (1) with the parameters $\alpha = 0.062$, $\mu = -0.61$, and $\sigma = 0.34$. The average grain size determined by the maximum of distribution (1) was found to be ~ 562 nm.

Figure 2. Image of the structure of a $Tm^{3+}:Lu_2O_3$ ceramic sample obtained with a scanning electron microscope with a magnification of 10^4.

The images recorded by the electron microscope show that the ceramics has a dense structure and the grains have an equiaxed shape and slightly differ in size. The grain sizes were calculated using the chord length measurement method [21]. We analysed eight regions of the ceramic sample, the number of analysed crystallites in each region being no less than 80. The grain size distribution is well approximated by a log-normal distribution function of the form

Figure 3. Normalised grain size distribution $f(d)$ calculated by the ceramic surface images obtained with a scanning electron microscope. The envelope is plotted using approximating function (1).

Figure 4. Two-dimensional (a) and three-dimensional (b) AFM-images of the ceramic surface after etching.
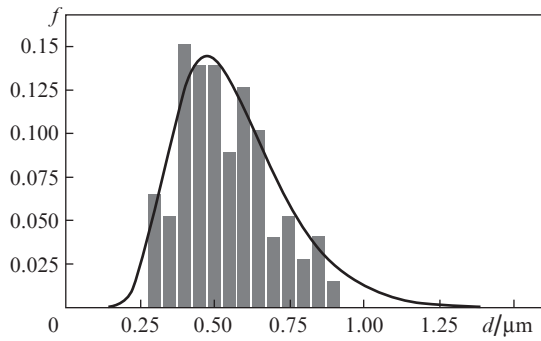
Figure 5. Normalised grain-size distribution $f(d)$ found from the AFM images of the ceramic surface. The envelope is plotted using approximating function (1).

Figure 6. Absorption spectrum of $Tm^{3+}:Lu_2O_3$ ceramics measured with a step of 0.2 nm.

Figure 7. Absorption spectrum of $Tm^{3+}:Lu_2O_3$ ceramics measured with a step of 0.1 nm (*1*) and absorption spectrum of a $Tm^{3+}:Lu_2O_3$ crystal calculated by the literature data [1] (*2*).

Figure 8. Transmission spectrum of $Tm^{3+}:Lu_2O_3$ ceramics in the near-IR region.

It should be noted that, except for grain boundaries, we did not observe other structural defects (inclusions, local formations, or pores) in the studied samples using both the scanning electron microscope and the AFM. Based on the images obtained by the electron microscope and AFM, we may conclude that the characteristic size of pores at the crystallite boundary is more than two orders of magnitude smaller than the characteristic grain size. However, the finite resolution of our devices does not allow us to estimate the sizes of boundary pores more precisely.

Note that the average grain size (~ 0.5 μm) estimated by the AFM images within the rms deviation coincides with the estimate obtained by processing the electron-microscope image. These estimates correspond to the concept of optimum crystallite sizes desired by producers of sesquioxide ceramics [22]. The submicron size of grains and the nanometer size of boundary pores lead to low scattering losses of IR light in ceramics [23, 24]. We can also note that the size of crystallites in the $Tm^{3+}:Lu_2O_3$ ceramics considerably differs from the size of crystallites in the best samples of $Y_3Al_5O_{12}$ ceramics, which varies from a few to tens micrometers (see, from example, [24–26]).
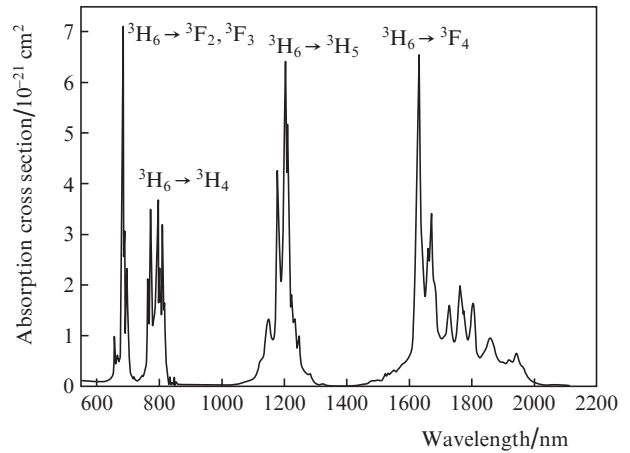
4. Study of the absorption spectrum

The absorption spectrum of $Tm^{3+}:Lu_2O_3$ ceramics within the range $\lambda = 500-2500$ nm was measured by a Perkin-Elmer Lambda 9 (Perkin-Elmer Inc.) spectrophotometer with a step of 0.2 nm. Based on our measurements of the sample transmittance $T(\lambda)$ and taking into account the Fresnel losses (with the coefficient F), we calculated the absorption cross section σ_{abs} (on the assumption of the absence of saturation) by the formula

$$\sigma_{abs} = \frac{\ln[F/T(\lambda)]}{N_0 l}, \qquad (2)$$

where N_0 is the concentration of Tm^{3+} ions (5.8×10^{20} cm^{-3} [1]) and l is the sample thickness (3 mm). The absorption spectrum measured at room temperature exhibits absorption lines from the ground $^3H_6$ state of the Tm^{3+} ion (Fig. 6).
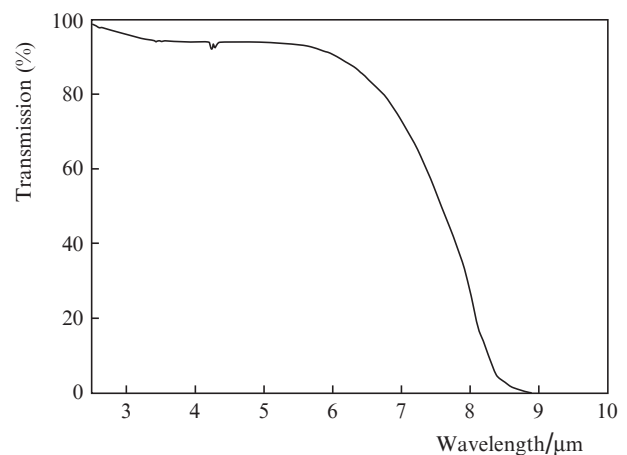
In the range of pump wavelengths (700–900 nm), we performed additional measurements with a step of 0.1 nm. Using the measurement results, we calculated by formula (2) the absorption cross section σ_{abs} to be 3.8×10^{-21} cm^2 in the peak at $\lambda = 796$ nm and 3.2×10^{-21} cm^2 in the peak at $\lambda = 811$ nm. Comparing the measured absorption spectrum of the ceramics
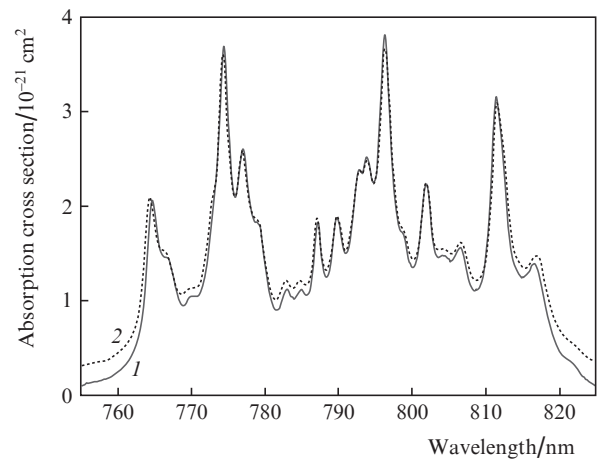
with the published data for $Tm^{3+}:Lu_2O_3$ crystals, one can see that they well coincide both in the positions and widths of the spectral maxima and in the absorption cross sections (Fig. 7).

Outside the absorption lines of Tm^{3+} ions, the ceramics transmission may be limited by scattering. The extinction coefficient (logarithmic scattering loss coefficient) in the studied sample was estimated to be smaller than 3×10^{-2} cm^{-1} (at $\lambda \sim 840$ nm).

Using an FTS-7000 (Digilab, now Varian) Fourier spectrometer, we studied the IR absorption spectrum of the ceramics in the region of $2.5-9$ μm (spectral resolution ~ 1 cm^{-1}) (Fig. 8). We used a DTGS detector with a Peltier cooling element. These measurements showed a high transmission of the ceramics at wavelengths $2.5-7$ μm.

5. Investigations of the luminescence spectrum

The luminescence spectrum of the $Tm^{3+}:Lu_2O_3$ ceramics under laser-diode pumping at $\lambda = 796$ nm (Fig. 9) was measured using an MDR-41 (LOMO, St. Petersburg, Russia) monochromator and an FSA-G1 photoresistor. The pump beam intensity during measurements did not exceed 100 W cm^{-2}, which excluded absorption saturation.
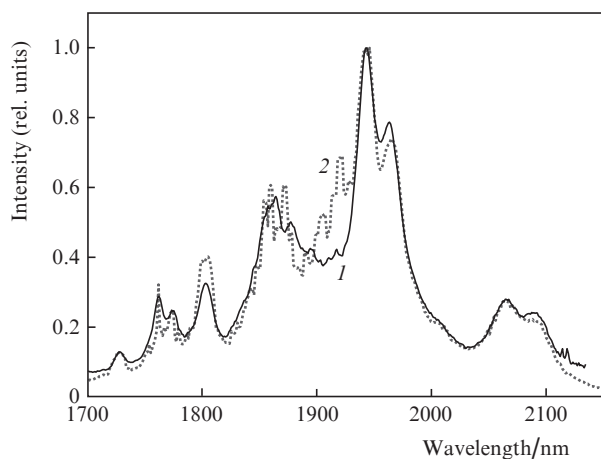

Figure 9. Luminescence spectra measured for the $Tm^{3+}:Lu_2O_3$ ceramics (1) and calculated for the $Tm^{3+}:Lu_2O_3$ crystal by the data from [1] (2).

In the range of $1.75-2.2$ μm, the luminescence spectrum of the ceramics pumped by a laser diode at $\lambda = 796$ nm contains strong lines peaked at $\lambda = 1942$, 1965, and 2066 nm. The positions and intensity ratios of these maxima coincide with the corresponding data for $Tm^{3+}:Y_3Al_5O_{12}$ crystals [7–10] with a good accuracy, restricted by the accuracy of digital reproduction of the literature data and by the accuracy of approximation of the detector frequency characteristic [compare curves (1) and (2) in Fig. 9]. It should be noted that the luminescence lines of the ceramics are smoother than the corresponding lines of the crystal. Similar difference in the luminescence lines near $\lambda = 2$ μm was also observed for the $Tm^{3+}:Y_3Al_5O_{12}$ ceramics and crystal, which was explained by an inhomogeneity of the Stark splitting of lines due to a difference in the electric fields inside crystallites and on their surfaces [26].

6. Study of the refractive index of $Tm^{3+}:Lu_2O_3$ ceramics with a spectroscopic ellipsometer

Using a PhE-102 (Micro Photonics Inc.) spectroscopic ellipsometer, we measured the refractive index of two ceramic samples in the range $\lambda = 300-1200$ nm with a resolution of
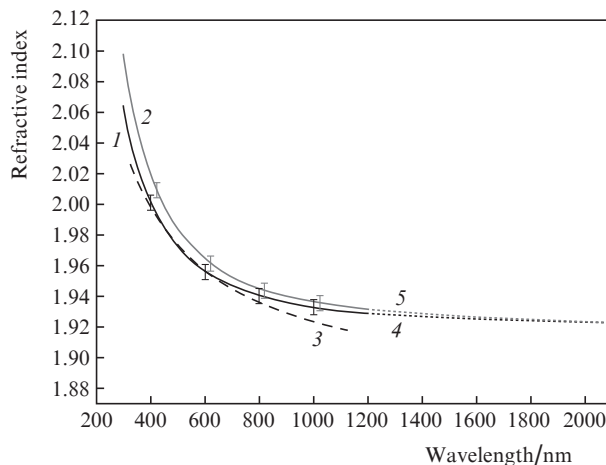
Figure 10. Wavelength dependence of the refractive index of $Tm^{3+}:Lu_2O_3$ ceramics measured with an ellipsometer for samples 1 (1) and 2 (2), plotted by the literature data (3), and approximated by the Sellmeier formula (3) for samples 1 (4) and 2 (5).

~ 1 nm (Fig. 10). The absolute measurement error did not exceed 0.005. We studied a $Tu^{3+}:Lu_2O_3$ ceramic plate (20 mm in diameter and 3 mm thick) without antireflection coating. The measured refractive index of the ceramics was compared with the literature data for Lu_2O_3 crystals [27]. To determine the refractive index at wavelengths of $1200-2100$ nm (outside the measurement region), we used the Cauchy approximation of the Sellmeier formula in the form [28]

$$n(\lambda) = \frac{A}{\lambda^2} + B\lambda^2 + C, \tag{3}$$

where A, B, and C are the fitting coefficients.

Using MATLAB software, we selected A, B, and C coefficients so that the difference between the approximation results and the measured data does not exceed 10^{-2}, namely $A = 1.3\times10^{-10}$ cm^2, $B = -1.256\times10^{-2}$ cm^{-2}, and $C = 1.92$ for sample 1 and $A = 1.6\times10^{-10}$ cm^2, $B = 1.033\times10^{-2}$ cm^{-2}, and $C = 1.92$ for sample 2.

The refractive index n at the pump radiation wavelength (~ 800 nm) was measured to be ~ 1.94. The approximation of its spectral dependence by formula (3) yields $n \approx 1.92$ at the laser wavelength ~ 2066 nm.

7. Study of lasing

We studied lasing in a specially prepared rod of $Tm^{3+}:Lu_2O_3$ ceramics (thulium concentration 2 at%) with a diameter of 3 mm and a length of 10 mm, whose faces were antireflection coated for the pump (~ 800 nm) and laser (~ 2066 nm) wavelengths. For better heat removal, the rod was wrapped in indium foil and mounted in a copper heatsink at a constant temperature of $\sim 12\,°C$.

The laser cavity was formed by three mirrors: two plane dichroic mirrors M1 and M2 with high ($\sim 99.9\%$) reflection coefficients for the region of $1.9-2.1$ μm (the transmittance of mirror M2 at the pump wavelength was $\sim 92\%$, and mirror M1 was highly reflecting for the pump radiation) and an output mirror M3, whose parameters were varied in the course of experiments (Fig. 11).

As a pump source, we used Coherent (US) or Jenoptik (Germany) fibre-coupled diode lasers operating at $\lambda = 796$ or
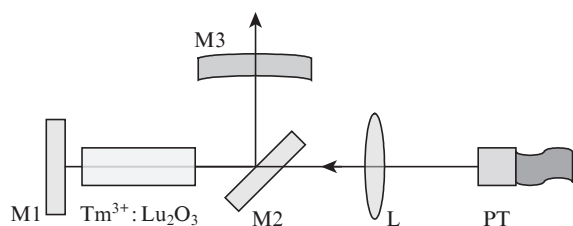
Figure 11. Scheme of the $Tm^{3+}:Lu_2O_3$ ceramic laser: (M1–M3) mirrors; (PT) pump laser pigtail; (L) lens system.
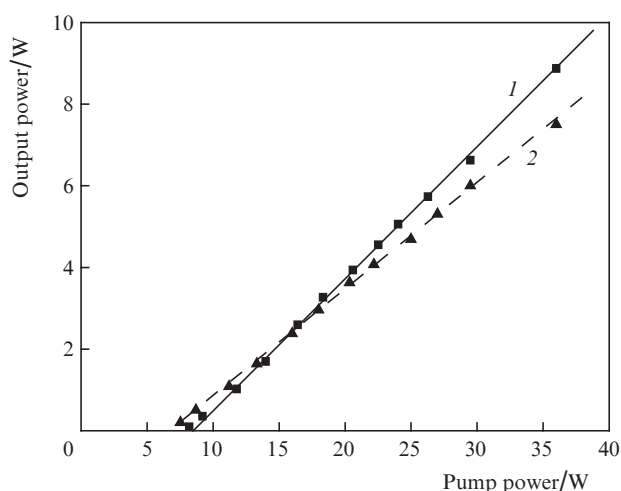
811 nm with the maximum output power up to 40 W. The pump radiation wavelength was tuned by changing the laser diode temperature to achieve the maximum output power. The diode array beam emitted from the multimode fibre face was focused through dichroic mirror M2 into the $Tm^{3+}:Lu_2O_3$ ceramic sample by a lens telescope consisting of a set of spherical lenses.

The output power of the $Tm^{3+}:Lu_2O_3$ laser was optimised by varying the cavity and pump beam parameters. In the scheme, we used output mirrors with different radii of curvature (∞, 200 and 300 nm) and transmittances (6% and 11%). The pump beam diameter in the active element was varied from 0.6 to 1 mm, and the position of its focal spot was moved to obtain the maximum output power.

Continuous-wave lasing was obtained in the case of pumping at both $\lambda = 796$ nm and $\lambda = 811$ nm (Fig. 12). The maximum output power of ~ 9.3 W (at a slope efficiency up to $\sim 40\%$) was achieved in the scheme with a plane output mirror (transmittance $\sim 11\%$), a beam waist diameter of ~ 800 µm, and the minimum possible cavity length (~ 6 cm). Our analysis of the output beam spectrum using an MDR-21 monochromator showed that, in all cases, lasing occurred in the long-wavelength region, at the 2066-nm line with a half-width of ~ 4 nm.

8. Conclusions

Thus, in this work we studied the structural, spectroscopic, and optical characteristics of $Tm^{3+}:Lu_2O_3$ laser ceramics. The average grain size was found to be ~ 0.5 µm with a dispersion of $150-200$ nm. We obtained cw lasing at $\lambda = 2066$ nm under pumping by diode lasers at $\lambda = 796$ and 811 nm. Our measurements allow us to conclude that the $Tm^{3+}:Lu_2O_3$ ceramics is promising for efficient high-power lasing in the two-micron wavelength region [29].

References

1. Scholle K., Lamrini S., Koopmann P., Fuhrberg P., in *2 µm Laser Sources and Their Possible Applications, Source: Frontiers in Guided Wave Optics and Optoelectronics* (Croatia, INTECH, 2010) Ch. 21, p. 471.
2. Grachev S. *Gol'mievyi laser v medicine* (Holmium laser in medicine) (Moscow: Triada-X, 2003).
3. Henderson S.W., Hale C.P., Magee J.R., Kavaya M.J., Huffaker A.V. *Opt. Lett.*, **16**, 773 (1991).
4. Budni P.A., Pomeranz L.A., Lemons M.L., Miller C.A., Mosto J.R., Chicklis E.P. *J. Opt. Soc. Am. B*, **17**, 723 (2000).
5. Walsh B.M. *Laser Phys.*, **19**, 855 (2009).
6. Moulton P.F., Rines G.A., Slobodtchikov E.V., Wall K.F., Frith G., Samson B., Carter A.L.G. *IEEE J. Sel. Top. Quantum Electron.*, **15**, 85 (2009).
7. Koopmann P., Lamrini S., Scholle K., Fuhrberg P., Petermann K., Huber G. *Techn. Dig. Conf. on Lasers and Electro-Optics 2010* (San Jose, USA, 2010) paper CMDD1.
8. Koopmann P., Lamrini S., Scholle K., Fuhrberg P., Petermann K., Huber G. *Techn. Dig. Int. Conf. «Advanced Solid-State Photonics»* (Istanbul, Turkey, 2011) paper ATuA5.
9. Koopmann P., Lamrini S., Scholle K., Fuhrberg P., Petermann K., Huber G. *Opt. Lett.*, **36**, 948 (2011).
10. Koopmann P., Peters R., Petermann K., Huber G. *Appl. Phys. B*, **102**, 19 (2011).
11. Lupei V., Lupei A., Ikesue A. *J. Alloys Compounds*, **380**, 61 (2004).
12. Lu J., Takaichi K., Shirakawa A., Musha M., Ueda K., Yagi H., Yanagitani T., Kaminskii A. *Appl. Phys. Lett.*, **81**, 4324 (2002).
13. Kaminskii A.A., Akchurin M.S., Gainutdinov R.V., Takaichi K., Shirakawa A., Yagi H., Yanagitani T., Ueda K.-I. *Crystallogr. Rep.*, **50**, 809 (2005).
14. Ueda K., Bisson J.-F., Yagi H., Takaichi K., Shirakawa A., Yanagitani T., Kaminskii A.A. *Laser Phys.*, **15**, 927 (2005).
15. Takaichi K., Yagi H., Shirakawa A., Ueda K., Hosokawa S., Yanagitani T., Kaminskii A.A. *Phys. Stat. Sol. (a)*, **202**, R1 (2005).
16. Tokurakawa M., Takaichi K., Shirakawa A., Ueda K., Yagi H., Hosokawa S., Yanagitani T., Kaminskii A.A. *Opt. Express*, **14** (26), 12832 (2006).
17. Bagaev S., Osipov V., Ivanov M., Solomonov V., Platonov V., Orlov A., Rasulaeva A., Vatnik S., Vedin I., Maiorov A., Pestryakov E., Shestakov A., Salkov A. *Fotonika*, **5**, 24 (2007).
18. Tokurakawa M., Shirakawa A., Ueda K.-I., Yagi H., Hosokawa S., Yanagitani T., Kaminskii A.A. *Opt. Lett.*, **33** (12), 1380 (2008).
19. Tokurakawa M., Shirakawa A., Ueda K., Yagi H., Meichin N., Yanagitani T., Kaminskii A.A. *Opt. Express*, **17** (5), 3354 (2009).
20. Newburgh G.A., Word-Daniels A., Arocksiamy M., Merkle L.D., Ikesue A., Dubinskii M. *Opt. Express*, **19** (4), 3604 (2011).
21. *GOST 5639-82. Stali i splavy. Metody vuyavleniya i opredeleniya velichiny zerna* (Steels and Alloys. Methods of grain detection and grain size determination) (Moscow: IPK 'Izdatel'stvo standartov', 2003).

Figure 12. Dependences of the laser output power on the diode pump power (incident to the active element) at $\lambda = 796$ (*1*) and 811 (*2*) nm.

22. Ballato J., Serivaisatit K. *Techn. Dig. Int. Conf. «Advanced Solid-State Photonics»* (Istanbul, Turkey, 2011) paper AIWA2.
23. Ikesue A., Aung Y.L., Taira T., Kamimura T., Yoshida K., Messing G.L. *Ann. Rev. Mater. Res.*, **36**, 397 (2006).
24. Boulesteix R., Maître A., Baumard J.-F., Rabinovitch Y., Reynaud F. *Opt. Express*, **18**, 14992 (2010).
25. Barmenkov Yu.N., Ivanov S.N., Taranov A.V., Khazanov E.N., Yagi H., Yanagitani T., Takaichi K., Bisson J.-F., Shirakawa A. *Pis'ma v Zh. Eksp. Teor. Fiz.*, **79**, 421 (2004).
26. Zhang Sh., Wang M., Xu L., Wang Y., Tang Yu., Cheng X., Chen W., Xu J., Jiang B., Pan Yu. *Opt. Express*, **19**, 727 (2011).
27. Ordin S.V., Shelykh A.I. *Fiz. Tekh. Polupr.*, **44**, 584 (2010).
28. Born M., Wolf E. *Principles of Optics* (New York: Pergamon Press, 1997).
29. Antipov O., Zakharov N., Novikov A., Sharkov V. *Techn. Dig. Europ. Conf. on Lasers and Electro-Optics CLEO/Europe 2011* (Munich, Germany, 2011) paper CA.P.21.